AD-A138 380 IMPEDANCE RELAXATION SPECTRUM ANALYSIS OF OXIDIZED 1/1
SILVER ELECTRODES(U) BROOKLYN COLL NY DEPT OF PHYSICS
M HEPEL ET AL. 31 JAN 84 TR-4 N00014-81-K-0399
UNCLASSIFIED F/G 9/1 NL

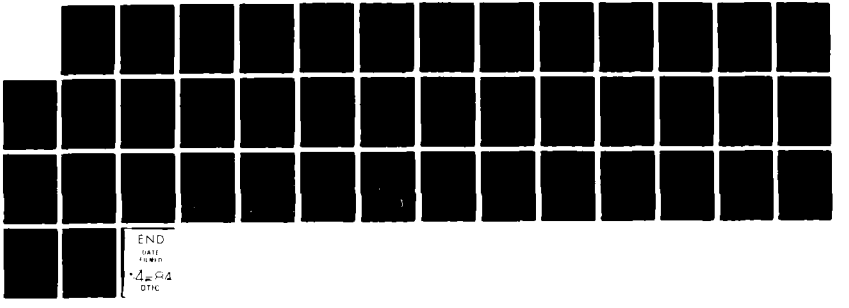

END
DATE FILMED
4-84
DTIC

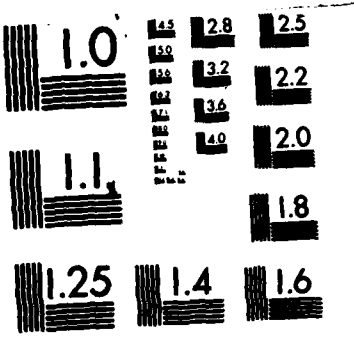

MICROCOPY RESOLUTION TEST CHART
NATIONAL BUREAU OF STANDARDS-1963-A

AD A138380

OFFICE OF NAVAL RESEARCH

Contract N00014-81-K-0399

Task No. NR - 628-765

TECHNICAL REPORT NO. 4

IMPEDANCE RELAXATION SPECTRUM ANALYSIS OF OXIDIZED SILVER ELECTRODES

by

Maria Hepel and Micha Tomkiewicz

Prepared for Publication

in

Journal of the Electrochemical Society

Physics Department, Brooklyn College of CUNY
Brooklyn, N. Y. 11210

January, 1984

Reproduction in whole or in part is permitted for any purpose of the United States Government

This document has been approved for public release and sale; its distribution is unlimited

DTIC ELECTE FEB 2 9 1984 A

DTIC FILE COPY

84 02 22 070

SECURITY CLASSIFICATION OF THIS PAGE (When Data Entered)

REPORT DOCUMENTATION PAGE

READ INSTRUCTIONS BEFORE COMPLETING FORM

1. REPORT NUMBER: 4	2. GOVT ACCESSION NO.: AD-A138 380
3. RECIPIENT'S CATALOG NUMBER:	
4. TITLE (and Subtitle): IMPEDANCE RELAXATION SPECTRUM ANALYSIS OF OXIDIZED SILVER ELECTRODES	5. TYPE OF REPORT & PERIOD COVERED:
	6. PERFORMING ORG. REPORT NUMBER:
7. AUTHOR(s): MARIA HEPEL MICHA TOMKIEWICZ	8. CONTRACT OR GRANT NUMBER(s): N00014-81-K-0399
9. PERFORMING ORGANIZATION NAME AND ADDRESS: PHYSICS DEPARTMENT BROOKLYN COLLEGE OF CUNY BROOKLYN, N. Y. 11210	10. PROGRAM ELEMENT, PROJECT, TASK AREA & WORK UNIT NUMBERS: NR - 628 - 765
11. CONTROLLING OFFICE NAME AND ADDRESS: OFFICE OF NAVAL RESEARCH/CHEMISTRY ATTN: CODE 413, 800 N. QUINCY STREET ARLINGTON, VA. 22217	12. REPORT DATE: January 31, 1984 13. NUMBER OF PAGES: 32
14. MONITORING AGENCY NAME & ADDRESS (if different from Controlling Office):	15. SECURITY CLASS. (of this report): UNCLASSIFIED 15a. DECLASSIFICATION/DOWNGRADING SCHEDULE:

16. DISTRIBUTION STATEMENT (of this Report)

APPROVED FOR PUBLIC RELEASE
DISTRIBUTION UNLIMITED

17. DISTRIBUTION STATEMENT (of the abstract entered in Block 20, if different from Report)

18. SUPPLEMENTARY NOTES

PREPARED FOR PUBLICATION IN THE JOURNAL OF ELECTROCHEMICAL SOCIETY

19. KEY WORDS (Continue on reverse side if necessary and identify by block number)

IMPEDANCE, ANODE, FILMS, DISCHARGE

20. ABSTRACT (Continue on reverse side if necessary and identify by block number)

The real and imaginary parts of the impedance of the oxidation silver electrode in 1M KOH solutions, have been measured in a frequency range of $1 - 1.3 \times 10^7$ Hz.

When the electrode is oxidized at a potential when only Ag_2O is formed, we were able to isolate three passive elements: the high frequency capacitance and the high and low frequency resistances. On further oxidation, at a potential i

DD FORM 1 JAN 73 1473 EDITION OF 1 NOV 65 IS OBSOLETE
S/N 0102-LF-014-6601

SECURITY CLASSIFICATION OF THIS PAGE (When Data Entered)

which AgO can be formed, we were able to isolate five passive elements: two capacitive and three resistive Two of these elements were identified as originating from the Ag_2O layer. The functional dependence of all these elements on the amount of charge that is used for oxidation, reveals that the Ag_2O layer can be analyzed in terms of a single dielectricum in a parallel plate capacitor. Parameters such as thickness of the layer, resistivity of the material and roughness factor could be evaluated.

We have found that at the potential in which AgO is formed, significant fraction of the charge is being used for formation of Ag_2O.

DTIC COPY INSPECTED 2

Dist A1

IMPEDANCE RELAXATION SPECTRUM ANALYSIS OF OXIDIZED SILVER ELECTRODES

Maria Hepel and Micha Tomkiewicz

Department of Physics, Brooklyn College of CUNY
Brooklyn, N. Y. 11210

KEY WORDS: Impedance, Anode, Films, Discharge

ABSTRACT

The real and imaginary parts of the impedance of the oxidized silver electrode in 1M KOH solutions, have been measured in a frequency range of 1 - ~~1.3 x 10~~ Hz.

When the electrode is oxidized at a potential when only Ag_2O is formed, we were able to isolate three passive elements: the high frequency capacitance and the high and low frequency resistances. On further oxidation, at a potential in which AgO can be formed, we were able to isolate five passive elements: two capacitive and three resistive. Two of these elements were identified as originating from the Ag_2O layer. The functional dependence of all these elements on the amount of charge that is used for oxidation, reveals that the Ag_2O layer can be analyzed in terms of a single dielectricum in a parallel plate capacitor. Parameters such as thickness of the layer, resistivity of the material and roughness factor could be evaluated.

We have found that at the potential in which AgO is formed, significant fraction of the charge is being used for formation of Ag_2O.

INTRODUCTION

The electrochemical behavior of silver - silver oxide electrode has been extensively studied (1-7) because of the importance of electrochemical storage systems such as silver - zinc, silver - cadium, silver - iron and silver-hydrogen batteries. It is known (8) that in alkaline solutions, silver is oxidized in two steps. Upon initial oxidation Ag_2O is formed which can be further oxidized to AgO. Impedance measurements (3,9) in addition to more conventional electrochemical methods, were used extensively, to characterize the chemical and morphological mechanism of the oxidation process(10). The technique of Relaxation Spectrum Analysis in which the impedance is monitored over a wide frequency range and the results are portrayed in terms of a set of parallel, frequency independent, R-C elements, was used in the past to describe the potential distribution at the semiconductor electrolyte interface (11). Recently, the technique was extended to characterize the interface of metallic single crystal RuO_2, with aqueous electrolytes (12).

The principal condition under which one can apply this mode of interpretation to the frequency dispersion of the impedance of the interface, is that the faradaic components will be negligible during the impedance measurements Thus, if this condition is satisfied, the impedance measurments are used to monitor static characteristics of the interface and changes in these characteristics due to perturbation of the system prior to the impedance measurements. The correlation between the changes in the static characteristics and the perturbations which give rise to them, provide the tools for understanding certain aspects of the dynamics of the system. The generalized equivalent circuit, which is based on a network of parallel R-C elements and which was so useful for the simple interfaces is clearly not appropriate for the study of the oxidation of the silver electrode.

Ag_2O is a small band gap (1.2 eV at 293°K (13)) semiconductor which is insulating with resistivities of the order of 10^6 - 10^8 Ωcm at room temperature (14). Although its electronic properties are not as well characterized as those of the better known semiconductors, and not even, as well, as the properties of its structural analoge, Cu_2O, there is no known methods of doping this material to reduce its resistivity to the region in which its semiconducting properties will dominate.

Our knowledge of the solid state properties of AgO are even less complete then that of Ag_2O. Since it was impossible to grow stable single crystals of this material. There is still an uncertainty whether the material have peroxide structure in the form of Ag_2O_2 or it actually represents higher oxidation state of the silver. It was characterized as an n type semiconductor, with a bandgap of ~2 eV (15). Unlike for Ag_2O, its resistivity can be reduced considerably down to a level of ~ 10 Ωcm (17,18). Since these two oxides vary so much in their transport properties it is natural that zero order interpretation of the impedance data should assume their separate contributions to the transport properties in series with each other. This simplified assumption should result in two possible R-C elements connected in series. If, on the other hand, AgO is formed not by direct oxidation of Ag_2O at the oxide electrolyte interface, but instead through nucleation, then a random distribution of the two oxides may be expected. Such a random distribution can not be analyzed in terms of well defined, dielectric materials connected in series, but rather as a changing dielectric constant of a random composite that can be analyzed by utilizing effective medium theories (19) that can calculate the frequency distribution of the dielectric constant of the composite as a function of its changing composition.

In this paper, we present evidence, that under certain experimental conditions, the evolution of the two oxides can be separately monitored. We present evidence that at least Ag_2O behaves as a pure dielectricum with

frequency independent dielectric constant and we follow the growth of Ag_2O as it is being further oxidized to AgO.

EXPERIMENTAL

Apparatus

The experimental set-up for impedance measurments was similar to the one described elsewhere (11). It consisted of a Hewlett-Packard 3320-B frequency synthesizer, 3575-A gain-phase meter and dc-bias supply. The system control and data aquisition were performed by a Hewlett-Packard Model 9830A micro-computer. The experimental data, relative magnitude M and phase shift Φ between the two input signals (impedance of the reference circuit and total impedance), were processed and analyzed by a computer interactive program. The electronic equipment used allowed for measurements up to the frequency 13 MHz, a limit practically unavailable for potentiostatic systems.

On the other hand, special precautions concerning the electrochemical cell design (similarly as in case of the bridge methods) had to be undertaken. Although, balancing the reference impedance and the cell impedance is not required for the method to be used, a comparable value of the reference impedance was always maintained in order to achieve the best accuracy of readings. The parasitic inductance of leads has been diagnosed and all the results presented here are corrected for the high-frequency inductance effects.

Electrochemical cell and materials

The electrochemical cell used for measurements was a standard two-compartment plexiglass cell of a capacity 100 cm^3. The counter electrode was made from a large graphite cylinder. A double-junction saturated (KCI) silver/silver chloride electrode with 1M KNO_3 external solution was used as a reference electrode. A high purity silver rod substrate (Johnson-Matthews, 99.99%) with an exposed surface area 0.385 cm^2 was used as a working electrode. The oxides films were prepared on this substrate according to a procedure

described below.

All chemicals used were of analytical grade purity. De-ionized water (18 Mohm) was obtained using Mili-Q purification system.

Experimental procedure

The polycrystalline silver substrate electrodes were polished to a mirror like surface using alumina with 0.03 μm grains. The surface was subsequently degreased in acetone and propyl alchohol, etched in diluted HNO_3 solution, rinsed with de-ionized water and dried in air. The bi-layer electrodes were prepared in two steps. During the first step an Ag_2O film was deposited in 1 mol/dm^3 KOH solution at constant potential E = + 300 mV (vs. Ag/AgCl double-junction reference electrode) using standard electrochemical equipment (a Model EG & G 173 potentiostat, equipped with a Model 179 digital coulometer and Model 175 universal programmer.) The deposition was carried out for several hours and was interrupted after a given charge had been passed through the cell. Then the electrode potential was increased to + 600 mV, to the region of the AgO formation. The deposition was carried out for different times allowing for a growth of the oxide films of different thicknesses. The anodic charge consumed in the second step was from 0.47 C to 15.1 C. The electrodes obtained in this way were then subsequently used in the impedance measurements with the network analyzer set-up described above.

All the solutions used were deoxygenated by passing argon. During the experiments an argon purge was maintained.

Results and Discussions

Figure 1 shows the cyclic voltamogram of oxidation and reduction of the silver/silver oxides electrode with the arrows indicating at which potentials the films were oxidized and the potentials at which the impedance of the system was measured. Figure 2 shows the impedance spectrum of the system when only Ag_2O is deposited and Figure 3 shows the impedance spectrum with 0.44C used for Ag_2O depostion, following by further oxidation to form AgO.

Similar data were taken for different amounts of deposition charge.

Next a generalized way of analyzing these results will be presented, followed by a detailed account of the Ag/Ag_2O and $Ag/Ag_2O/AgO$ systems.

1. Relaxation Spectrum Analysis in a series presentation

If the generalized equivalent circuit of the system is presented as series of passive R-C elements like the one shown in Figure 4(a), with R_s, the series resistance due to the electrolyte, r_s^i - the series resistance of phase i and C_p^i and R_p^i the capacitance and shunt resistance of phase i. If phase i behaves like an insulator then $r_s^i = 0$ and C_p^i and R_p^i will relate, through the geometry of the system and the frequency, to the real and imaginary parts of the dielectric constant. If, on the other hand, phase i behaves like a semiconductor with space charge layer which is small compared to the thickness of the material, then only r_s^i relates to the resistivity of the system and C_p^i and R_p^i will relate to the charge distribution at the space charge layer and will vary with the potential drop across phase i. The impedance of such an equivalent circuit is given by:

$$Z = R + jX = R_s + \sum_i Z^i \tag{1}$$

where R and X are the real and imaginary components of the impedance.

$$Z^i = r_s^i + \frac{R_p^i}{1 + j\omega\tau^i} = r_s^i + \frac{R_p^i}{1 + (\omega\tau^i)^2} - J\frac{\omega R_p^i \tau^i}{1 + (\omega\tau^i)^2} \tag{2}$$

where ω is the angular frequency and $\tau^i = R_p^i C_p^i$, the relaxation time characteristic of phase i. Substituting eq. (2) in eq. (1) we will obtain the following expressions for the real and imaginary parts of the total impedance:

$$R = R_s + \sum_i r_s^i + \sum_i \frac{R_p^i}{1 + (\omega\tau^i)^2} \quad (3)$$

$$X = -\omega \sum_i \frac{R_p^i \tau^i}{1 + (\omega\tau^i)^2} \quad (4)$$

Thus, as in the parallel case, a function can be formulated, in this case simply by the imaginary part of the impedance, in which one obtains a line shape which is superimposition of Lorentzians type peaks. If the various contributions can be resolved, then the number of peaks will indicate the number of components i, and each peak will be centered at $\omega = \frac{1}{\tau_i}$ and X at the maximum will be equal to $R_p^i/2$, from which one can readily evaluate C_p^i and R_p^i.

From the high frequency components of the real part one can evaluate $R_s + \sum_i r_s^i$. The individual r_s^i can not be evaluated by this technique.

Figure 3 shows the impedance spectra, when both Ag_2O and AgO are present. The imaginary part of the impedance, even in the logarithmic scale, shows clearly two main peaks. It remains to be established whether either of these peaks is due to a single relaxing, passive, R-C element, but clearly the procedure that was established here offers the best starting point.

Figure 2, shows the impedance spectra when only Ag_2O is present, it does not show any resolvable peaks in the imaginary part. The behavior here, resembles the one observed with single phase interfaces and which was analyzed (11) in terms of a network of parallel RC elements as shown in Fig. 4b. We will not attempt full analysis of the network here and will concentrate only on the fastest relaxing RC element and the shunt resistance R(0).

It should be emphasized that the analysis of the data in terms of parallel or series networks is not unique and is a matter of convenience only. It serves primarily to isolate charge accumulation modes according to their relaxation times.

2. Ag/Ag_2O System

Under the conditions in which Relaxation Spectrum Analysis on parallel

network can be performed, there exists a frequency region in which the equivalent circuit can be reduced to a single R-C element(11). In this frequency range, the impedance is given by:

$$Z_{HF} = R - \frac{j}{\omega C_f} \qquad (5)$$

In this region

$$\log (2\pi X) = - \log f - \log C_f \qquad (6)$$

and log(2πX) should be linear with log f with a slope of -1 and an intercept from which C_f can be extracted. The real part, is frequency independent and equal to R_s, the series resistance of the system. From Fig. 2, the frequency range of 8000 - 800000 Hz satisfy these criteria (curve III in Fig. 2). The exact frequency domain in which these criteria are met varies from experiment to experiment. For each experiment the entire frequency dispersion of the impedance was measured, the frequency domain with the fastest relaxing R-C element was identified and the resistance and capacitance values measured. The variations of these parameters with the amount of charge that was passed to oxidize silver to Ag_2O will be discussed in this section. The oxidation was done at a constant potential of 0.3 V vs. Ag/AgCl with different oxidation times and the measurements were taken at the rest potential which has changed little in the limits 0.19 - 0.24 V vs. Ag/AgCl with increasing film thickness. For each experiment the electrode was freshly polished.

Figure 5 shows the results of the dependence of $1/C_f$ on the oxidation charge Q. Figure 6 shows the dependence of R_s on Q which was taken from the high frequency component of R, the same figure also shows the dependence on Q of R(1), the real part of the impedance at low frequency. The spread in the data is considerable, nevertheless a few qualitative conclusions can be drawn:

(1) R_s is independent of Q and can be shown to be dominated by the resistance of the electrolyte.

(2) C_f decreases as Q increases while R(1) remains approximately constant with a large spread of the data.

If we attempt to treat the system as a parallel plate capacitor in which Ag_2O

serves as the dielectricum and further assume a unit Faradaic efficiency for formation of Ag_2O then:

$$Q = \frac{2FdYA\ell}{M} \tag{7}$$

where F is the Faradaic number, d - the density, A - the geometric area, ℓ - the thickness of the capacitor and Υ - the roughness factor and M - the molecule weight of Ag_2O. The capacitance will be given by:

$$C = \frac{\varepsilon_o \varepsilon \Upsilon A}{\ell} \tag{8}$$

where ε is the dielectric constant and ε_o is the permittivity of free space. The resistance, R_T, which is associated with this dielectricum is given by:

$$R_T = \frac{\rho \ell}{\Upsilon A} \tag{9}$$

where ρ is the resistivity of Ag_2O. Substituting ℓ from (7) into (8) and (9) one gets:

$$\frac{1}{C_T} = \frac{MQ}{2Fd\varepsilon\varepsilon_o A^2 \Upsilon^2} \tag{10}$$

$$R_T = \frac{\rho MQ}{2FdA^2\Upsilon^2} \tag{11}$$

These equations predict linear behavior of $\frac{1}{C_T}$ and R_T with respect to Q and they predi also that $\tau = R_T C_T = \rho\varepsilon\varepsilon_o$ is independent of the geometric factor involved.

The data from Fig. 5 can be analyzed in terms of equation (10) after correcting for C_e, the capacitive element on the electrolyte side of the interface, such that:

$$\frac{1}{C_f} = \frac{1}{C_T} + \frac{1}{C_e} \tag{12}$$

Analysis of Fig. 5 in terms of equations (10) and (12) yields intercept of $8 \times 10^5 F^{-1}$, slope of $8.5 \times 10^6 C^{-1} F^{-1}$ with correlation coefficient of 0.92.

The dielectric constant of Ag_2O is not reported in the literature, but the variations in similar solids (oxides and non-oxides) are all within the range of 5 - 10. If we take the dielectric constant of Ag_2O to be similar to that of Cu_2O which is its structural analog, then $\varepsilon \approx 7$. Taking $d = 7.44 g/cm^3$, $M = 232$ and $A = 0.385 cm^2$, one can calculate from the slope of Fig. 5 and from equation (10) that $\gamma = 14$ and from the intercept we obtain: $C_e = 3.2 \times 10^{-6} F/cm^2$ if one considers the capacitance/geometric area and $C_e = 2.3 \times 10^{-7} F/cm^2$ if one takes into account the roughness factor. These values are on the low side of the capacitance of the Helmholtz layer, but the quality of the data and the assumptions in the model makes further speculations unwarranted.

If, at least qualitatively, the data in Fig. 5 could be analyzed in terms of equation (10) it is obvious that the data in Figure (6) can not be analyzed in terms of equation (11). R(1) does not represent R_T. We will return to the possible characterization of R(1) in the next section. At this stage, since we do not possess, as yet, information about the resistive component across the oxide, we can not evaluate the relaxation time of the material. Hence, we can not evaluate its resistivity.

3. $Ag/Ag_2O/AgO$ System

For this set of experiments the amount of charge, used for Ag_2O formation was kept constant at 0.44C. We then increased the potential to E = 0.600 V vs. Ag/AgCl, where AgO formation takes place (see Fig. 1). We have measured the impedance at the rest potential of Ag_2O/AgO which is 0.450 V vs Ag/AgCl. We have measured the impedance as a function of the amount of charge that was used for deposition of AgO. Figure 3 shows a typical result of such a measurement. As was mentioned in section 1, even on a logarithmic scale, two peaks, one at high frequency and the other at low frequencies, can be seen. The procedure that was developed in section 1 will be used as a basis for interpreting the

results. The first step in this process is to establish whether either of these peaks is due to a single relaxing, passive, R-C element. Examination of the low frequency peak in Fig. 3 clearly shows that the peak is too broad for a single Lorentzian. Figure 7 shows the evolution of the frequency dispersion of the imaginary part of the impedance with the amount of charge that was used to form the oxide. The amplitude of the high frequency peak increases in direct proportion to the deposition charge, while the high frequency tail of the low frequency peak is little affected by the deposition. Figure 8 shows the numerical fit of the high frequency peak to a normalized single Lorentzian. Except at the tail ends of the peak where inductance dominate on the high side and low frequency contributions on the low side, the fit is very good and the peak will be treated as a single Lorentzian.

As was mentioned before the low frequency peak is much too broad for a single Lorentzian. We do not want here to speculate about the various processes that might contribute to this peak. Figure 7 shows that the high frequency tail of this peak remains constant with deposition charge. It will be useful to determine whether this high frequency tail corresponds to a single passive R-C element. From eq. (4), the contributions of a single Lorentzian to the imaginary part of the impedance is given by:

$$X^i = - \frac{\omega R_p^i \tau^i}{1 + (\omega\tau^i)^2} \qquad (13)$$

The high frequency tail of this peak is defined for $\omega\tau^i >> 1$. Under these conditions:

$$X^i = - 1/\omega C_p^i \qquad (14)$$

and the analysis will be similar to the high frequency component of the parallel case which was used in section (2).

Figure 9 shows the fit between the experimental points at the high frequency tail of the low frequency peak and equation (14). The fit is good for nearly two orders of magnitude of frequencies. From the intercept of this

curve:

$$Cp = 4.10^{-5}\ F \equiv 1.0 \times 10^{-4}\ F/cm^2$$

based on the geometric area of the electrode.

Based on the absolute value of C_p and particularly observation that it is nearly independent of the amount of AgO deposition or Ag_2O growth during the deposition of AgO, it is reasonable to interpret this capacitive element, to be due to the junction between AgO and the electrolyte. It can be dominated by the capacitance of the Helmholtz layer, or by that of the space charge layer in the conductive oxide or by combination of the two. As long as the width of the space charge layer is smaller than the thickness of the oxide, the value of the capacitance will be independent of charge.

Let us now turn our attention to the fastest relaxing R-C element. Figures 10 and 11 show the variation of $1/C_f$ and R_f with the amount of charge Q_1 associated with deposition at 0.6 V on top of 0.44 C associated with Ag_2O that was deposited at 0.3 V vs Ag/AgCl. Figures 10 and 11 show that both R_f and $\frac{1}{C_f}$ increase with Q_1, where Q_1 is the total amount of charge deposited at 0.6 V vs. Ag/AgCl, then they both saturate at $Q_1 > 5C$. If we neglect the low coverage (up to 0.5C) where nucleation is known to take place, the functional dependence can be represented by:

$$\frac{1}{C_f} = \frac{5.6 \times 10^7 Q_1}{1 + 1.1\, Q_1} \qquad (15)$$

$$R_f = \frac{187 Q_1}{1 + 0.67\, Q_1} \qquad (16)$$

The inserts in both figures show the fit of the experimental points to this presentation from which the constants in equations (15) and (16) were evaluated If we take the saturation in both R_f and C_f to indicate saturation in the formation of the dielectric material that is responsible for the high frequency peak, then, within the parallel plate approximation:

$$\tau = (R_f C_f)_{sat} \approx 5.10^{-6} sec = \rho \varepsilon \varepsilon_o \qquad (17)$$

Taking again, as in (2) $\varepsilon = 7$, we obtain $\rho \simeq 8.2 \times 10^6$ Ωcm.

The high resistivity can only be due to Ag_2O. We arrive here to the conclusion that at the potential at which we form AgO, the characteristics of the Ag_2O layer changes as well. If AgO is being formed by oxidation of Ag_2O whose thickness does not increase the expected changes would have been the exact opposite to the one actually observed. We would have expected the Ag_2O layer to decrease in thickness with oxidation which would have resulted in decrease in resistance and increase in the capacitance of the layer. The observed results in Figures 10 and 11 can be interpreted in two ways: either at this potential both oxides are formed and if AgO is being formed by oxidation of Ag_2O, it implies that Ag_2O is formed by oxidation of silver faster then it is being oxidized, or alternatively, the high electric field and the deposition of AgO on top of the Ag_2O film results in "electroannealing" of the Ag_2O film which will considerably decrease the resistivity of the film. We prefer the first interpretation on two grounds: (1) We do not see two kinds of Ag_2O, unless one is willing to accept the idea that the "old" Ag_2O have moved to the low frequency peak. This would have required reduction of few orders of magnitude in the resistivity of Ag_2O lower than any recorded value for this parameter. (2) According to the "electroannealing" argument, the variation of C_f and R_f with Q is due only to the time spent at the anodic potential. Under galvanostatic conditions $Q \sim t$ and it would have been difficult to determine which of these two parameters is the key factor. However, the experiment here was performed under potentiostatic conditions in which the current was time dependent and as a result Q was not linear with t. From equations (15) and (16), in a limited range of Q, both R_f and $1/C_f$ are linear with Q which makes the direct correlation with time highly

improbable.

Assuming, as a result, that Figures 10 and 11 indicate continuous deposition of Ag_2O while Ag_2O is being further oxidized to AgO, we will try to analyze the correlation between R_f and $1/C_f$ with Q in a manner similar to the one that was explored in section 2. Let us assume that fraction α of the charge, Q_1, was used for the oxidation of Ag_2O to AgO and the remaining charge was used for the oxidation of Ag to Ag_2O. The net amount of charge used for deposition of new Ag_2O is given by:

$$Q_{net} = (1-2\alpha)\, Q_1 \tag{18}$$

Following the arguments that led to equations (10) and (11) in section (2), the capacitance and resistance of the newly formed Ag_2O layer will be given by:

$$\frac{1}{C_f} = \frac{n(1-2\alpha)Q_1}{2Fd\varepsilon\varepsilon_o A^2\gamma^2} + \frac{1}{C_f^o} \tag{19}$$

$$R_f = \frac{\rho M(1-\alpha)\, Q_1}{2FdA^2\gamma^2} + R_f^o \tag{20}$$

where C_f^o and R_f^o are the values for $Q_1 = 0$.

Comparing equations (15) and (16) with (19) and (20) prior to saturation one can evaluate $\gamma/\sqrt{1-2\alpha}$ this implies that if we can evaluate the roughness factor in an independent experiment then the ratio between the two oxidation reactions can be evaluated. From equations (19) and (15) one can calculate that $\gamma / \sqrt{1-2\alpha} = 15.3$.

Up to now we have evaluated all the data that we could extract from the frequency dispersion of the imaginary part of the impedance. From Figure 3 one can observe that at both ends of the frequency spectrum, the real part of the impedance is frequency independent. Fig. 12 shows the dependence of the high frequency component, $R(\infty)$ and the low frequency component, $R(1)$, as a function of deposition charge. The high frequency component resembles the behavior that was shown in Fig. 6, when only Ag_2O was present and is consistent with the interpretation that was made there, that $R(\infty)$ is due to the series resistance, R_s, which is due to the electrolyte. $R(1)$ on the other hand, increases with deposition charge in a manner which resembles R_f in Fig. 11. However, the absolute values are considerably smaller than the R_f values. This is in sharp contradiction with equation (2) which demands that:

$$R(0) = \lim_{\omega \to 0} R = R_s + \Sigma r_s^i + \sum_i R_p^i \qquad (21)$$

Since R_f is one component of this sum, equation (21) requires that $R(0) > R_f$. Since the low frequency part of the imaginary part of the impedance was shown to result from multiplicity of unresolved processes, we do not feel secure in proposing a definite pathway for these frequencies. More work is needed, before some definite conclusion about the low frequency regime can emerge.

CONCLUSIONS

We have shown that impedance measurements can be used to gain information about the chemical and topological changes that take place during oxidation of the silver electrode. Distinction between perturbation and detection was the key in enabling us to interpret the results using the simplest possible model and to correlate the measurements with the perturbation in a straightforward way.

We have shown that the technique of Relaxation Spectrum Analysis, which separates the charge accumulation modes at simple interfaces, according to their relaxation times, expressed in terms of simple, frequency independent, RC elements, can be extended to systems in which to first approximation, the charge accumulation modes are in series with each other. Under conditions when only Ag_2O is deposited, the impedance spectra behaved as that of a single interface. We were able to extract three, well behaved, passive elements: the high frequency capacitance, the high frequency resistance and the low frequency resistance. We have tried to identify the physical origin of these elements by monitoring their dependence on the amount of charge that was used to oxidize the electrode. The resistive element was found to be independent of charge while the reciprocal of the capacitive element have increased in a linear way with the amount of charge. The functional dependence of the capacitive element on the amount of charge was consistent with a simple model of a parallel plate capacitor in which Ag_2O serves as the dielectric material. Based on this model an "average" roughness factor, which is independent of the thickness of the layer was

calculated and found to be ~ 14. Based on this model, we were able to determine that, at least for the conditions that were investigated here, Ag_2O behaves as an insulator in which the electric field is distributed across the entire sample and does not concentrate at the interface. The high frequency resistance was associated with the resistivity of the electrolyte, while the low frequency resistance was associated with kinetic effects. At the potential in which the silver can be oxidized to AgO, we were able to extract five well behaved, passive elements and to monitor their variation with the amount of deposited charge. We were able to isolate the capacitive and resistive elements of a single dielectricum . In terms of a parallel plate model, these two parameters relate to the real and imaginary parts of the dielectric constant of the material through the geometric factor of the capacitor. The relaxation time of this material was found to be $\approx 5.10^{-6}$ sec from which resistivity of ~ 8.10^6 Ω cm was evaluated. The high resistivity, clearly demonstrates that the material is still Ag_2O. The conclusion was that at the potential where silver can be oxidized to AgO, significant fraction of the charge goes for an increase in the thickness of the Ag_2O layer. For amount of charge in excess of ≈ 15 C/cm^2, the capacitive and resistive elements which are associated with the Ag_2O, saturate and a steady state is achieved between formation of Ag_2O and oxidation of Ag_2O to AgO.

Acknowledge:

This work was supported by the Office of Naval Research. The authors wish to thank Dr. Benedict Aurian-Blajeni for his helpful discussions.

References

1. S.U. Falk and A.J. Salkind, Alkaline Storage Batteries, John Wiley & Sons, 1969.
2. J.M.M. Droog and Fred Huisman, J. Electroanal. Chem., 115 (1980) 211.
3. B.W. Tilak, R.S. Perkins, H.A. Kozlowska and B.E. Conway, Electrochim. Acta, 17 (1972) 1447.
4. R.S. Perkins, B.V. Tilak, B.E. Conway and H.A. Kozlowska, Electrochim. Acta, 17, (1972) 1471.
5. B. Miller, J. Electrochem. Soc., 117 (1970) 491.
6. R. Memming, F. Mollers and G. Neumann, J. Electrochem. Soc., 117, (1970) 451.
7. M.L. Teijelo, Y.R. Vilche and A.J. Arvia, J. Electroanal. Chem., 131 (1982) 331.
8. C.P. Wales and J. Burbanek, J. Electrochem. Soc., 111 (1964) 1002; 106 (1959) 885.
9. B.G. Pound, D.D. Macdonald and J.W. Tomlinson, Electrochim. Acta, 27 (1982) 1489.
10. T.P. Hoar and C.K. Dyer, Electrochim. Acta, 17 (1972) 1563.
11. M. Tomkiewicz, J. Electrochem. Soc. 126 (1979) 2220.
12. M. Tomkiewicz, Y.S. Huang and F.H. Pollak, J. Electrochem. Soc., 130 (1983) 1514.
13. O. Madelung (Ed.), Landolt-Bornstein, New Series, Vol. 17, Springer-Verlag, Berlin 1983, p. 155.
14. E. Fortin and F.L. Weichman, Phys. Stat. Sol., 5 (1964) 515.
15. E. Farhat and S. Robin-Kandare, Thin Solid Films 23 (1974) 315.
16. A. Tvarusko, J. Electrochem. Soc., 115 (1968) 1105.

17. M. Le Blanc and H. Sachse, Z. Phys., 32 (1931) 887.

18. A.B. Naiding and J. A. Kazarnovskii, Dokl. Akad. Nauk SSSR, 78 (1951) 713.

19. D.E. Aspnes, Am. J. Phys. 50 (8) (1982) 704.

Figures

Figure 1. The CV characteristic for the polycrystalline silver electrode (geometric area A = 0.385 cm^2) in 1 mol dm^{-3} KOH solution at 22°C. V = 10 mV/s.

E'_{dep} and E''_{dep} are potentials of deposition of Ag_2O and AgO, respectively (used in further deposition experiments.)

E'_r and E''_r are the rest potentials at which impedance spectra were measured.

Figure 2. Impedance spectrum for a polycrystalline silver electrode covered by a thin film of Ag_2O deposited at E = +300 mV (vs. Ag/AgCl). (I) $Z = \log R_1$ (II) $-Q = \log (2\pi X)$, (III) $Q = -\log t - \log C_f$. Solution: 1 mol dm^{-3} KOH.

Figure 3. Impedance spectrum for a bilayer $Ag/Ag_2O/AgO$ electrode in 1 mol dm^{-3} KOH. Total deposition charge: 2.9 C/cm^2. (I) $Q = \log R$, (II) $Q = \log (2\pi X)$.

Figure 4. Generalized equivalent circuit for series (a) and parallel (b) configurations of the passive elements. R_p and C_p are the parallel resistance and capacitance, respectively, for the inner film (prime) and the interface (i); τ_s's stand for the respective time constants; R_s is the ohmic resistance mainly due to the electrolyte; R(0) is the low-frequency resistance; C_f is the film capacitance and C_i R_i are the series time constants.

Figure 5. Dependence of the reciprocal of the Ag_2O film capacitance $1/C_f$ determined from the impedance relaxation spectra upon the oxide-deposition charge Q. Coefficients of the linear fit to the experimental points are given.

Figure 6. Plot of the experimental data R_s and R(1) vs. deposition charge Q for the Ag/Ag_2O electrode in 1 mol dm^{-3} KOH solution.

Figure 7. Frequency dispersion of the imaginary part of the impedance of the bilayer $Ag/Ag_2O/AgO$ electrode in 1 mol dm^{-3} KOH at various AgO deposition charges [C]: (1) 0.91, (2) 1.05, (3) 1.19, (4) 1.48.

Figure 8. Computer fit of the high frequency reactance peak to a single Lorentzian for different AgO deposition charges [C]: (1) 0.91, (2) 1.05, (3) 1.19.

Figure 9. Fit of the high frequency tail of the low frequency peak to a single Lorentzian for the bilayer $Ag/Ag_2O/AgO$ electrode.

Figure 10. Dependence of the inner film capacitance C_f for the bi-layer $Ag/Ag_2O/AgO$ electrode in 1 mol dm^{-3} KOH upon the reciprocal of the oxide deposition charge 1/Q.

Figure 11. Plot of the reciprocal of the inner film resistance $1/R_f$ vs. $1/Q_1$ for the $Ag/Ag_2O/AgO$ layered electrode in 1 mol dm^{-3} KOH.

Figure 12. Dependence of $R(\infty)$ and R(1) upon the oxide deposition charge Q_1 for the bilayer $Ag/Ag_2O/AgO$ electrode in 1 mol dm^{-3} KOH.

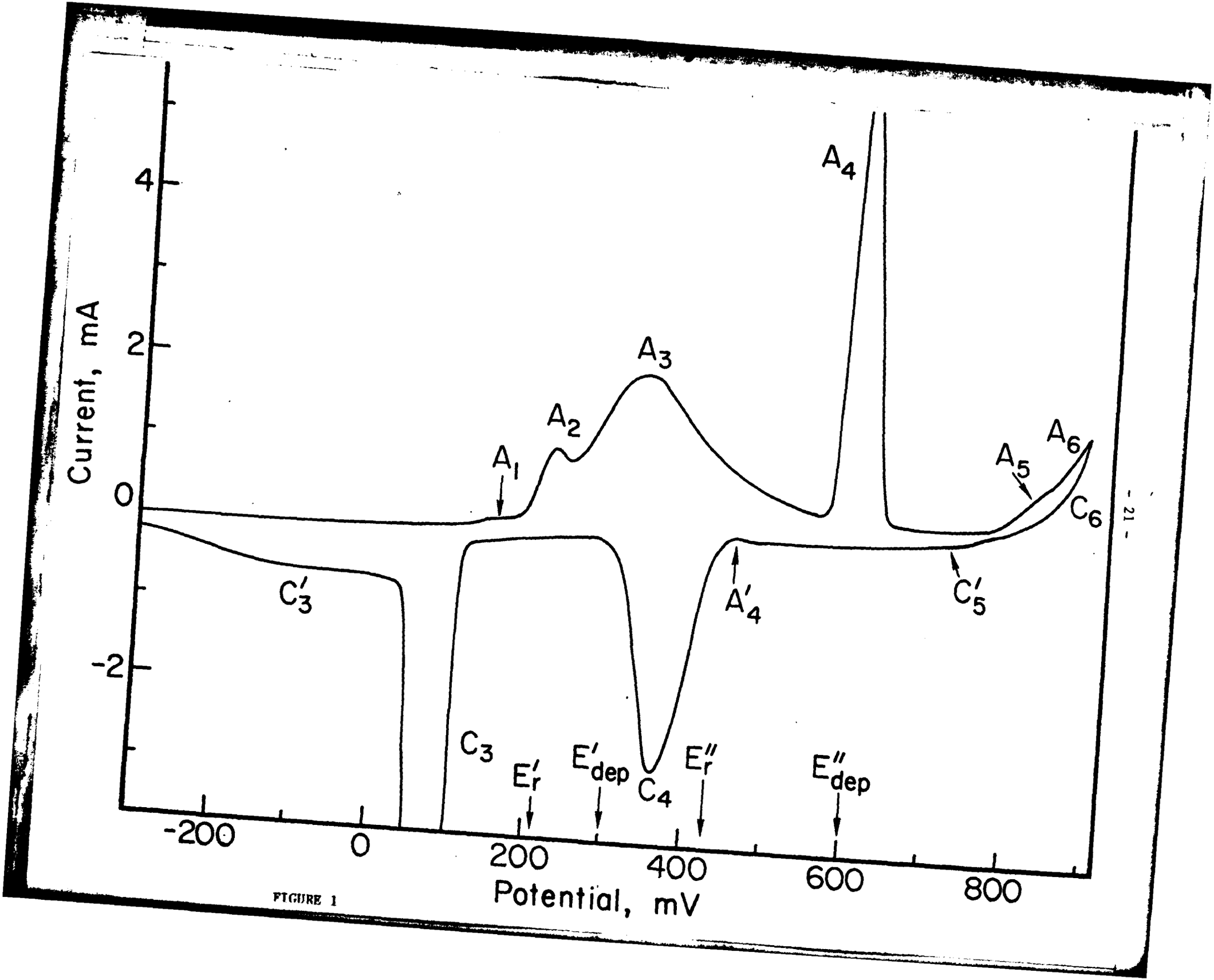
Current, mA
4
2
0
-2
A4
A3
A2
A1
A5
A6
C6
C'3
C'5
A'4
C3
E'r
E'dep
C4
E''r
E''dep
-200
0
200
400
600
800
Potential, mV

FIGURE 1

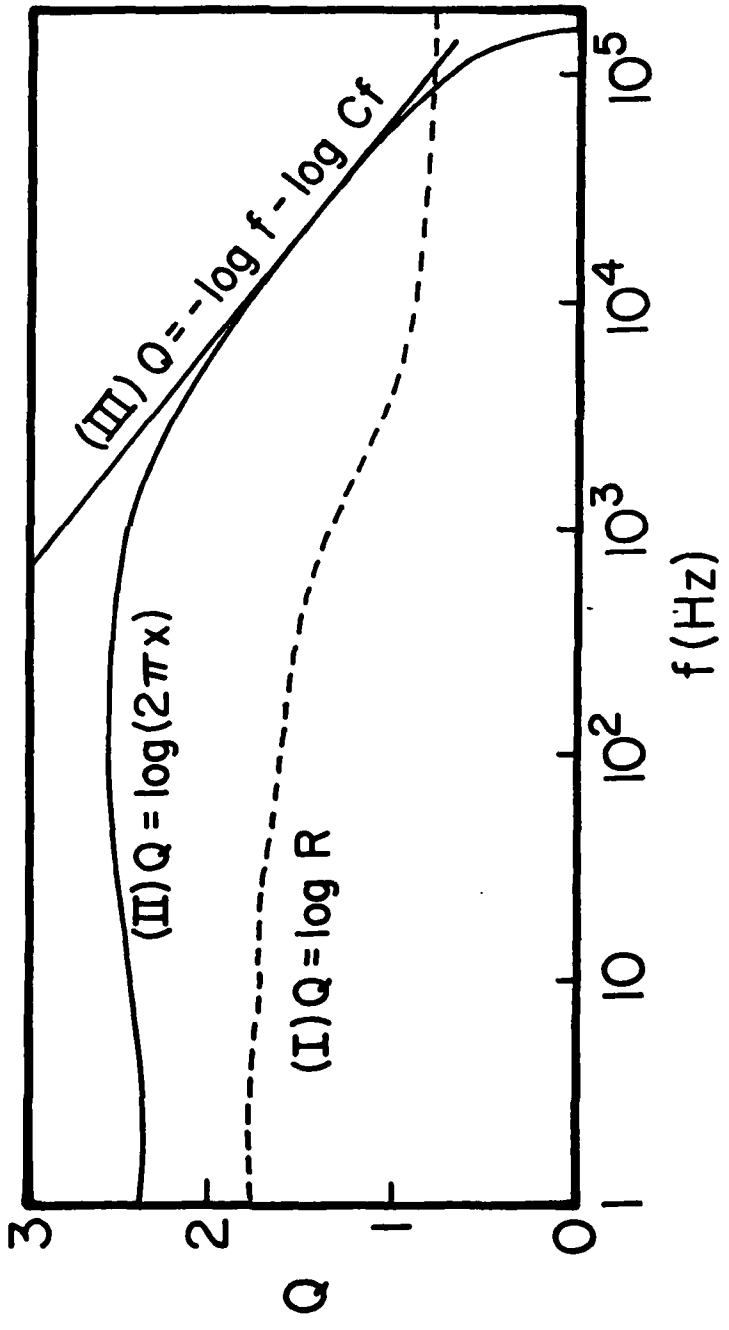
(III) Q = -log f - log Cf
(III) Q = log(2πx)
(I) Q = log R
Q
3
2
1
0
1
10
10²
10³
10⁴
10⁵
f (Hz)

FIGURE 2

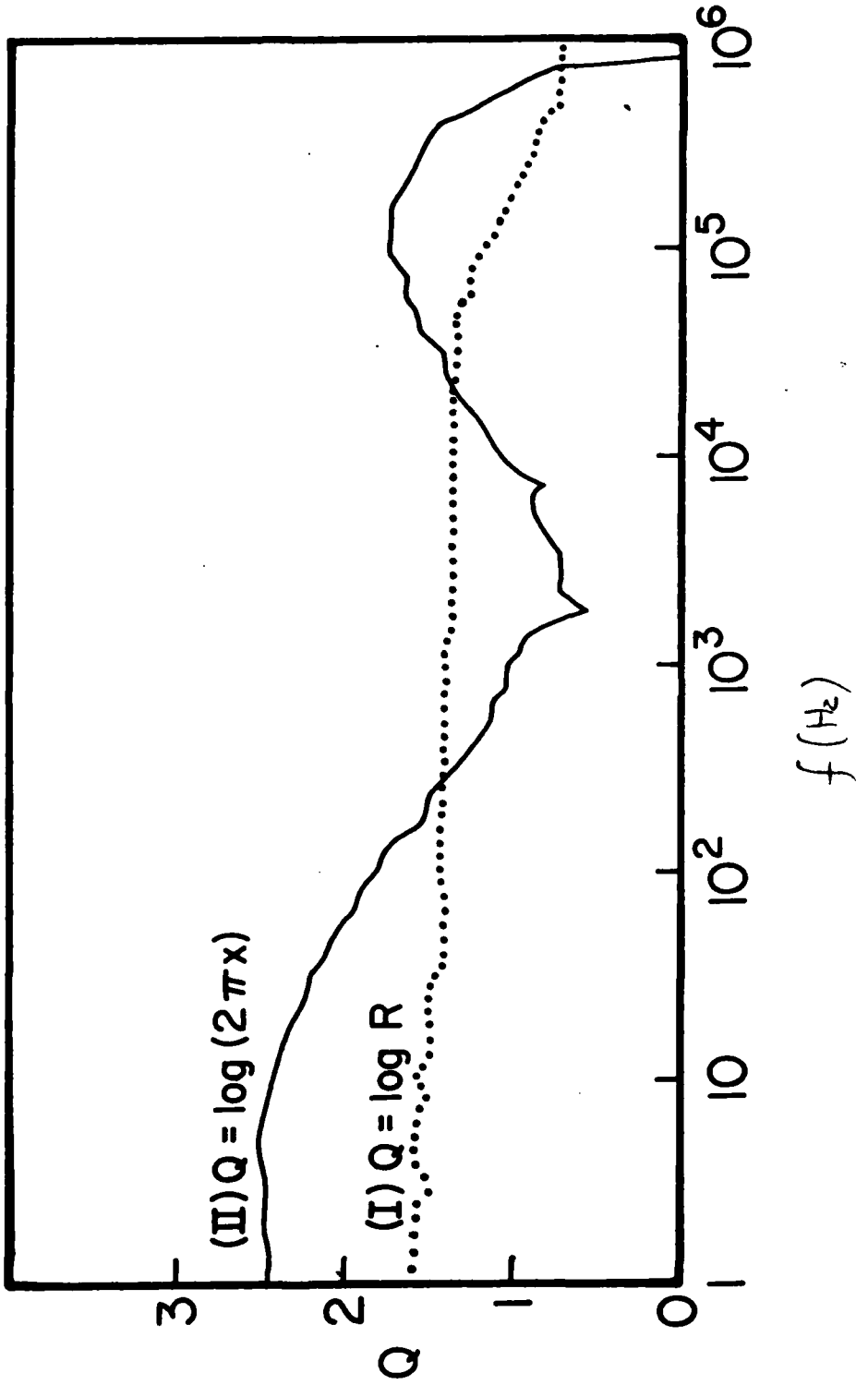

FIGURE 3

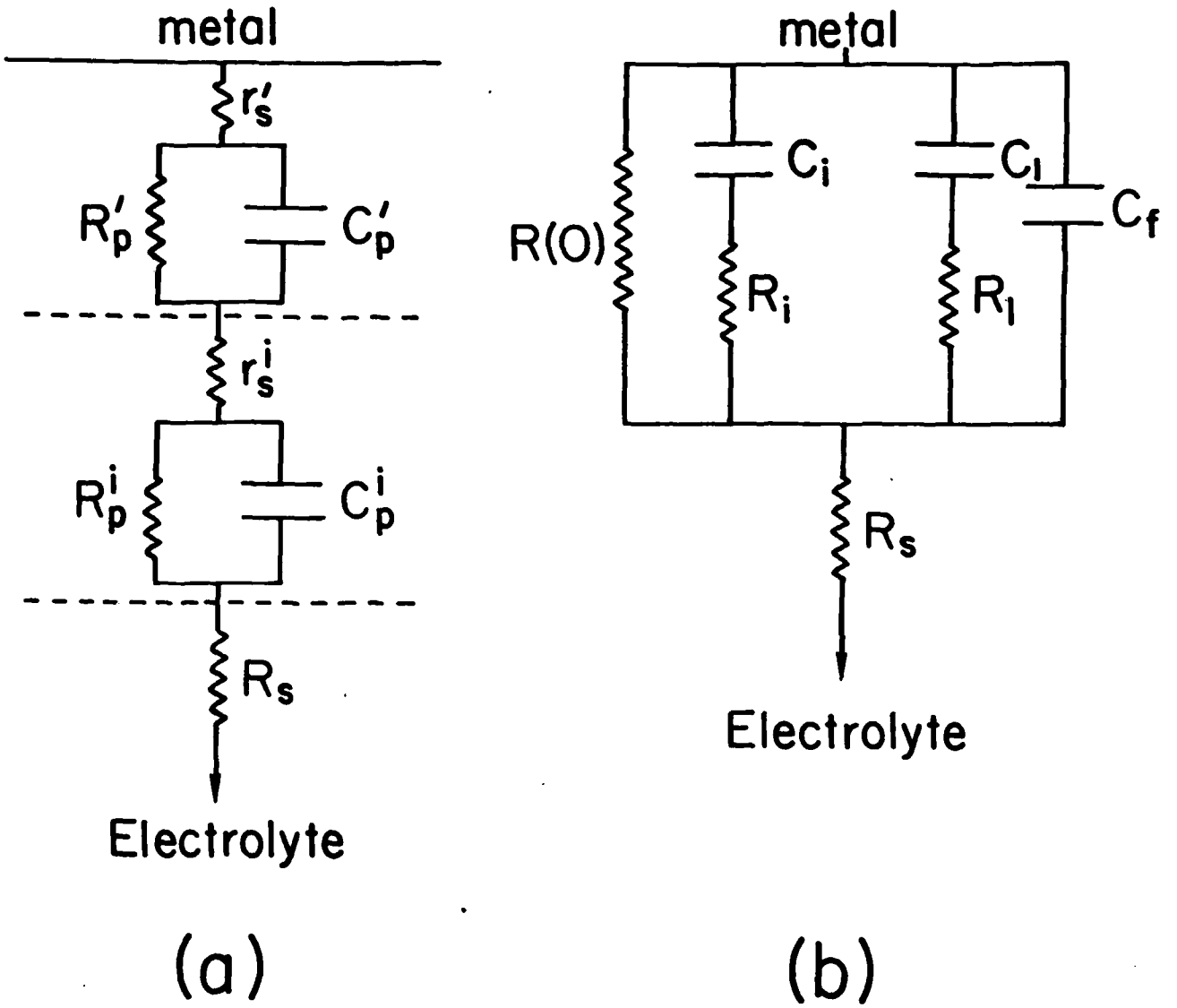
metal
r'_s
R'_p
C'_p
r^i_s
R^i_p
C^i_p
R_s
Electrolyte
(a)
metal
C_i
C_l
C_f
R(O)
R_i
R_l
R_s
Electrolyte
(b)

FIGURE 4

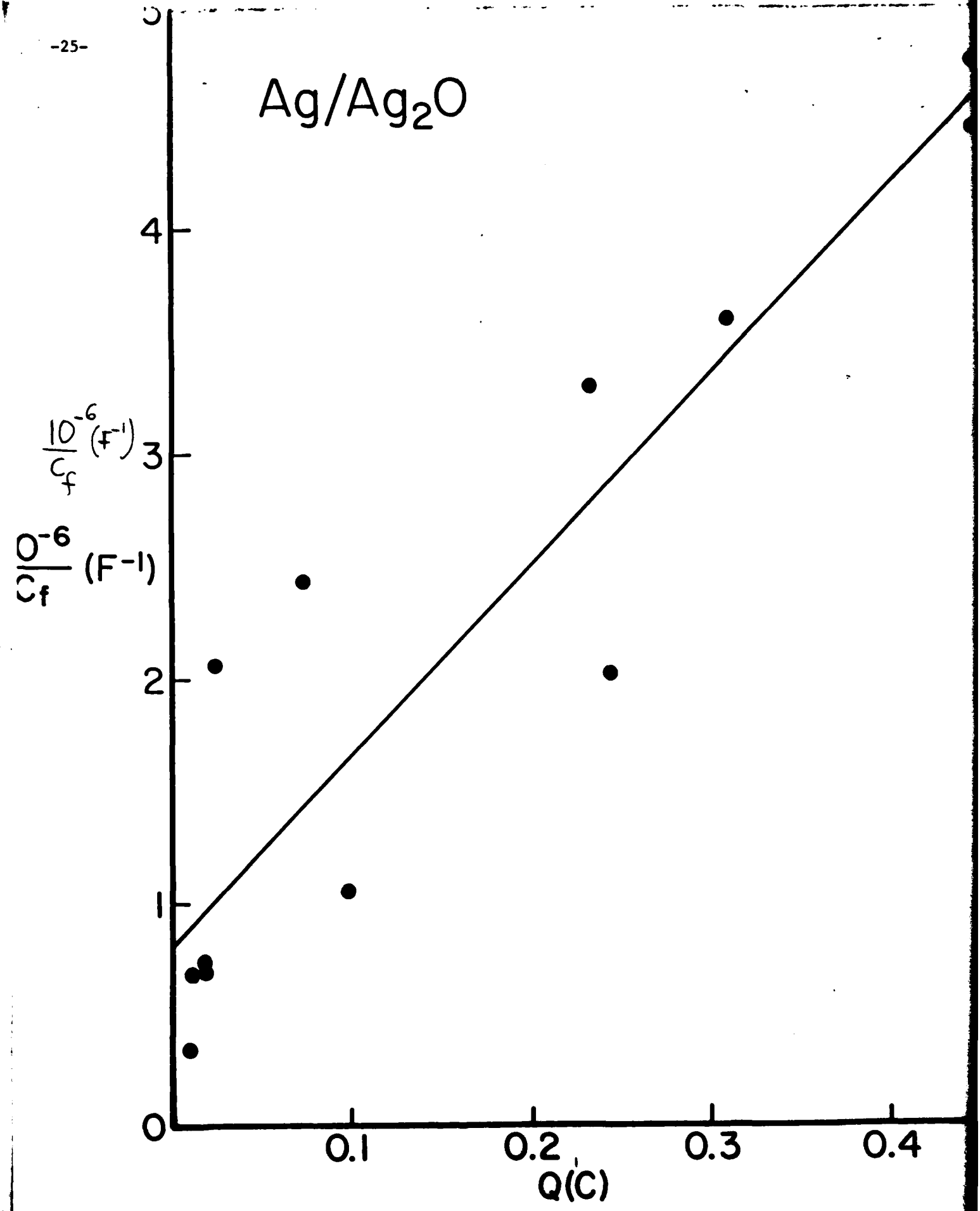

FIGURE 5

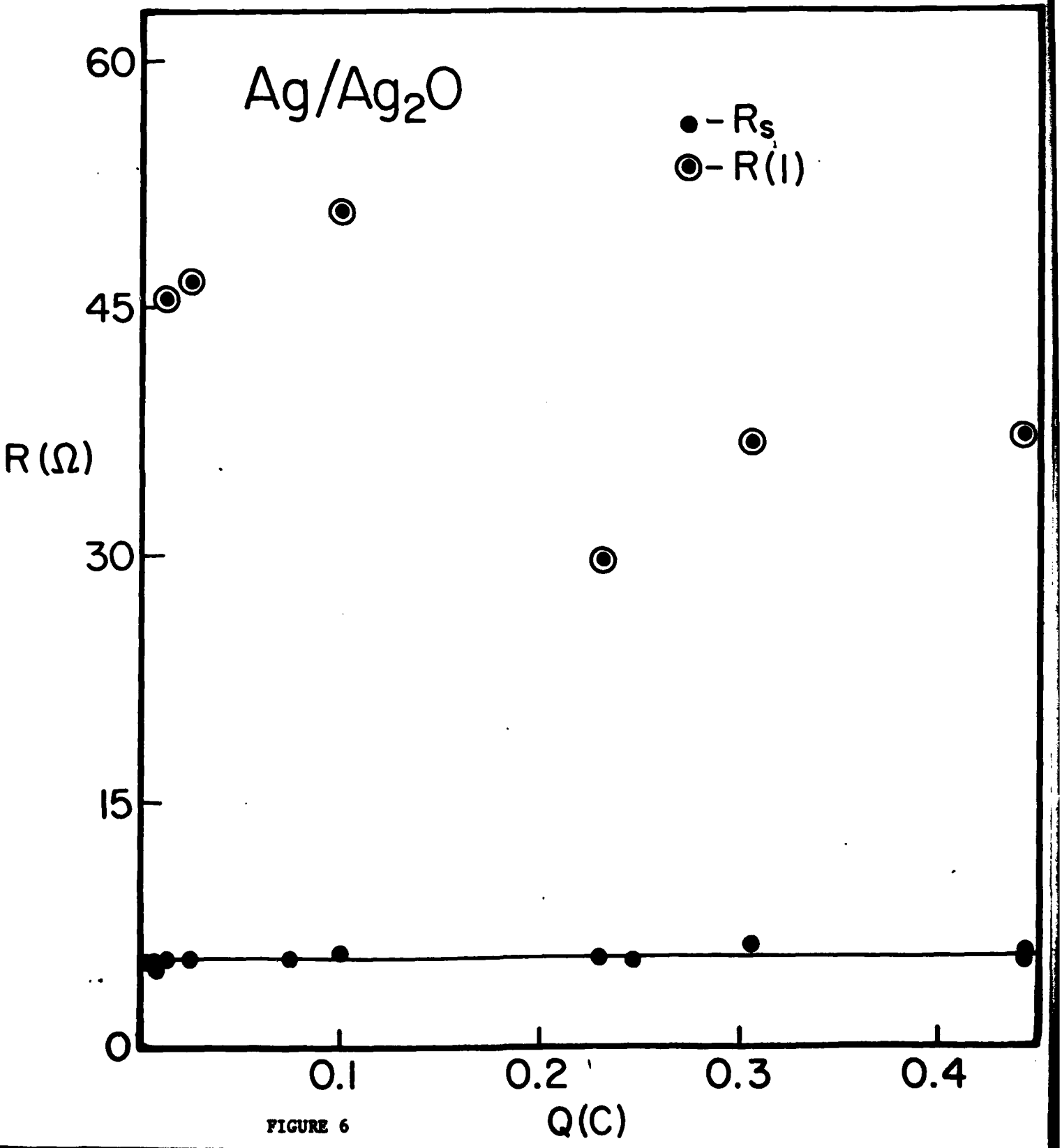

FIGURE 6

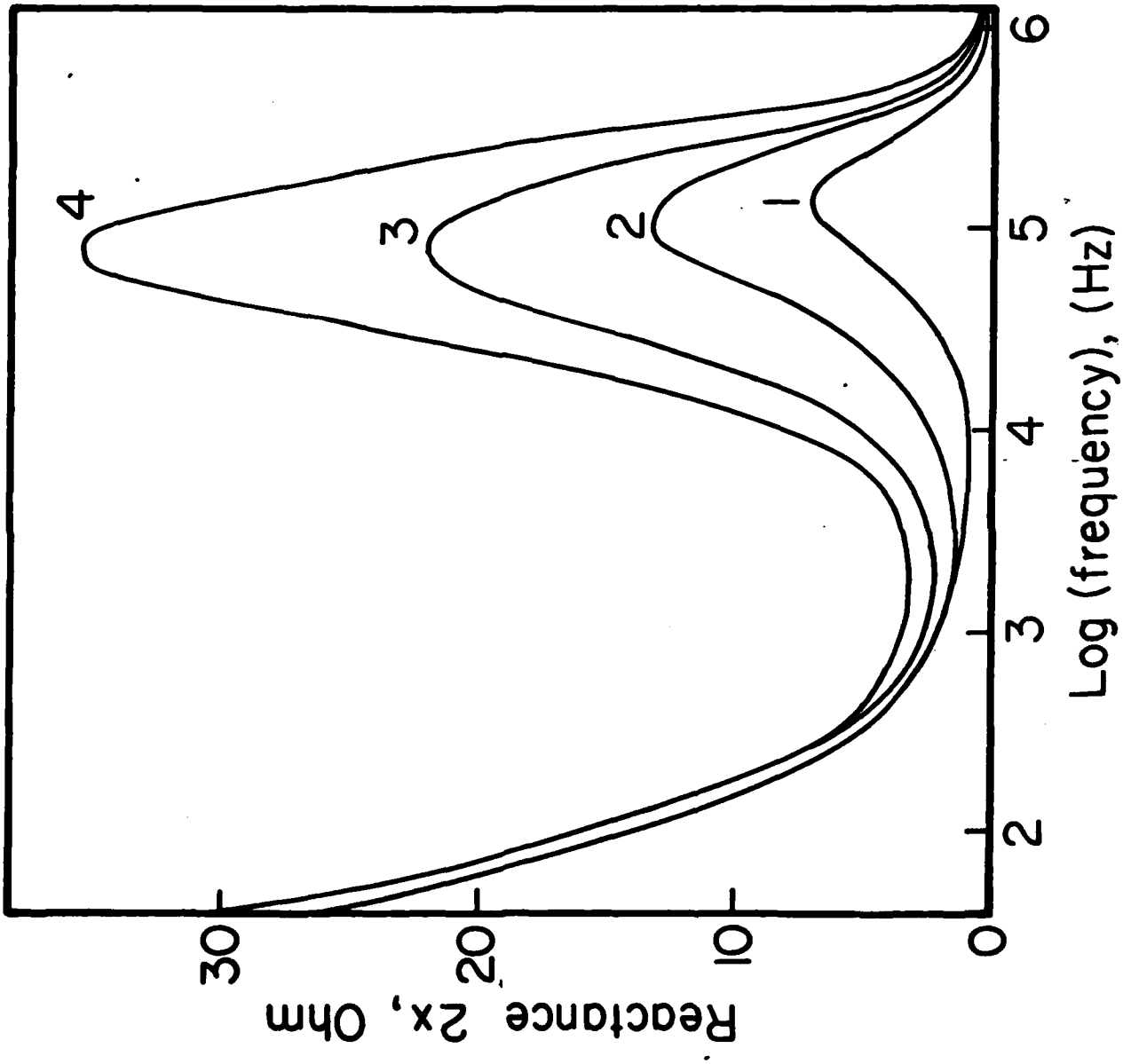
Reactance 2x, Ohm
30
20
10
0
2
3
4
5
6
Log (frequency), (Hz)
1
2
3
4

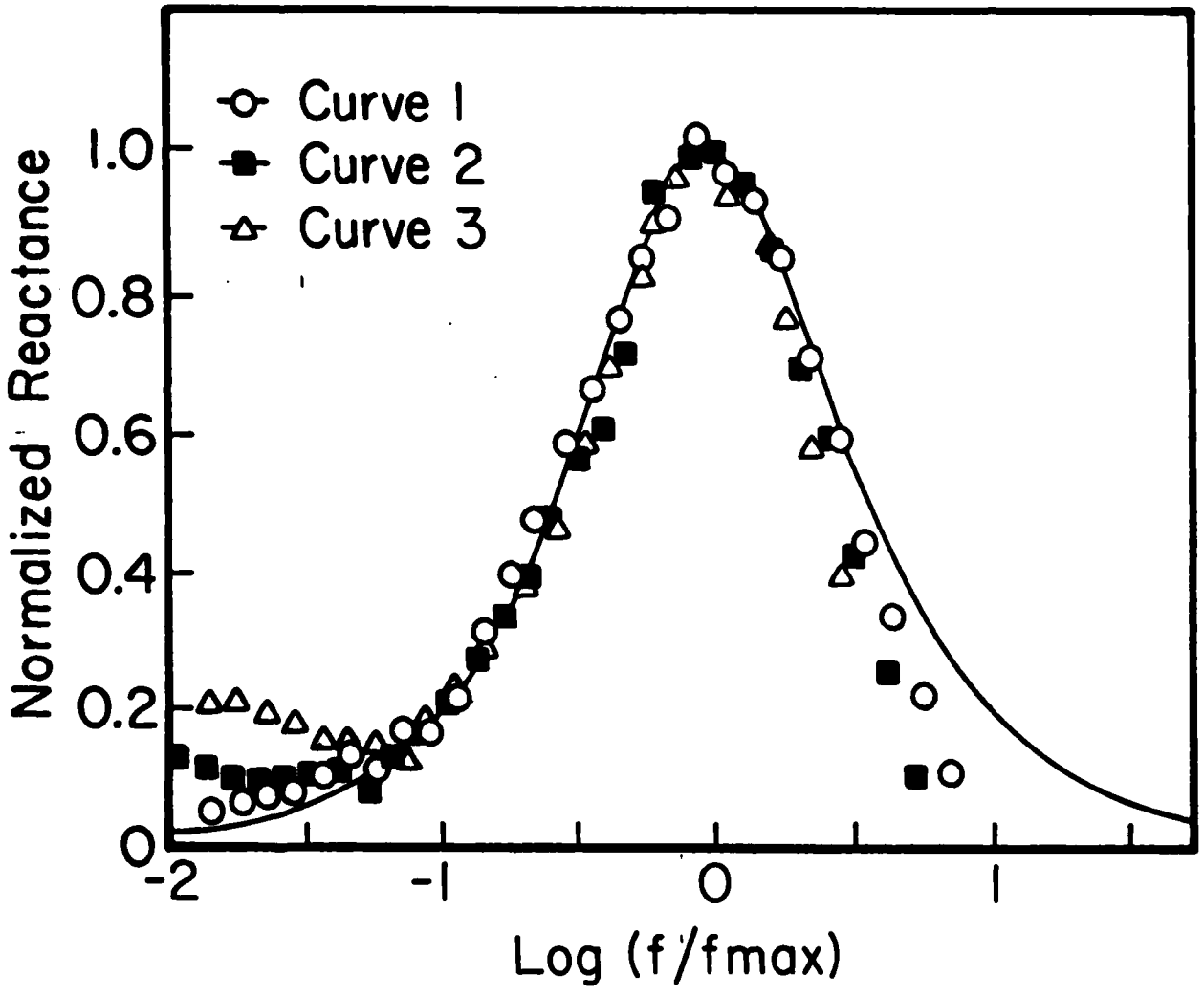
Curve 1
Curve 2
Curve 3
Normalized Reactance
1.0
0.8
0.6
0.4
0.2
0
-2
-1
0
1
Log (f/fmax)

FIGURE 8

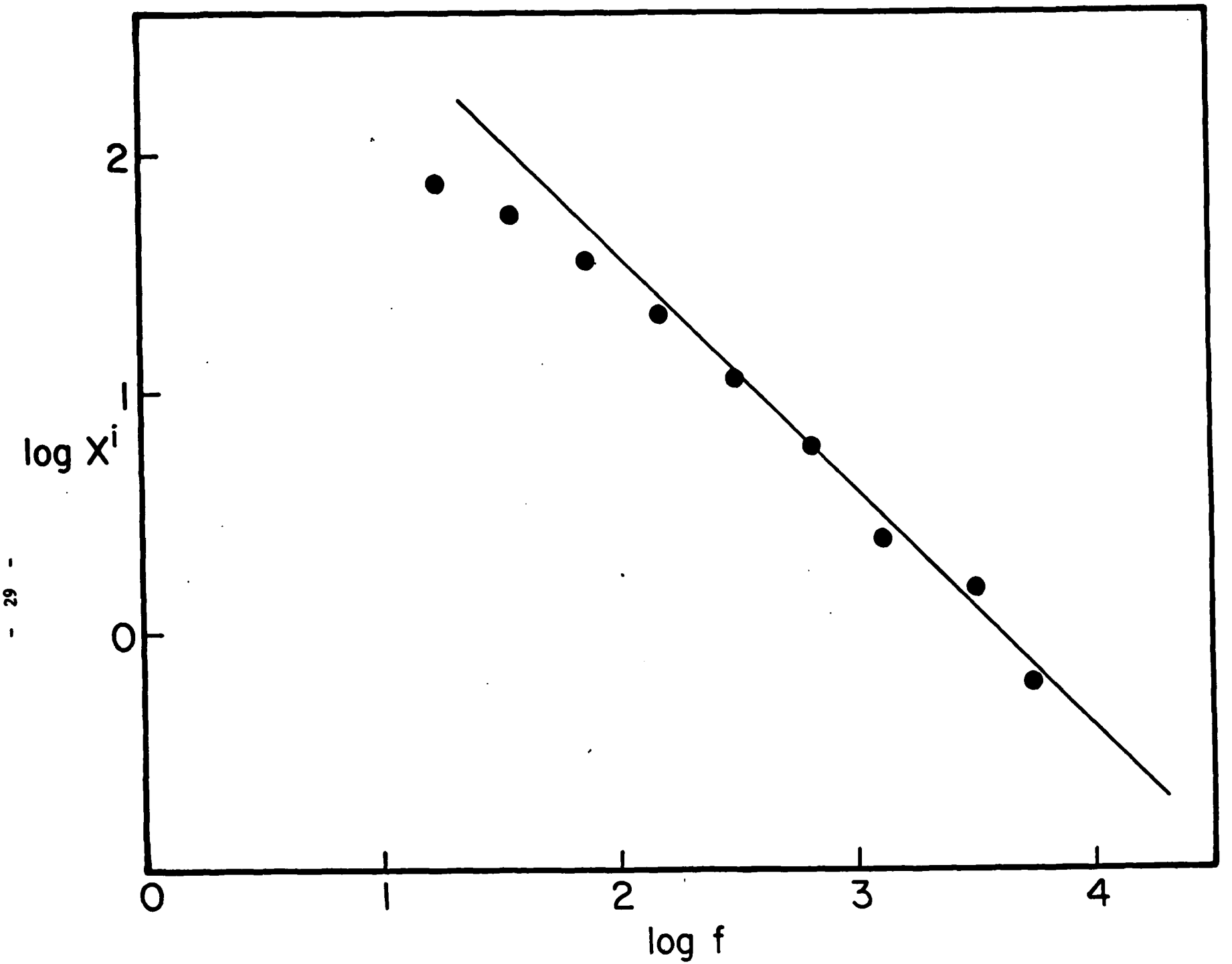

FIGURE 9

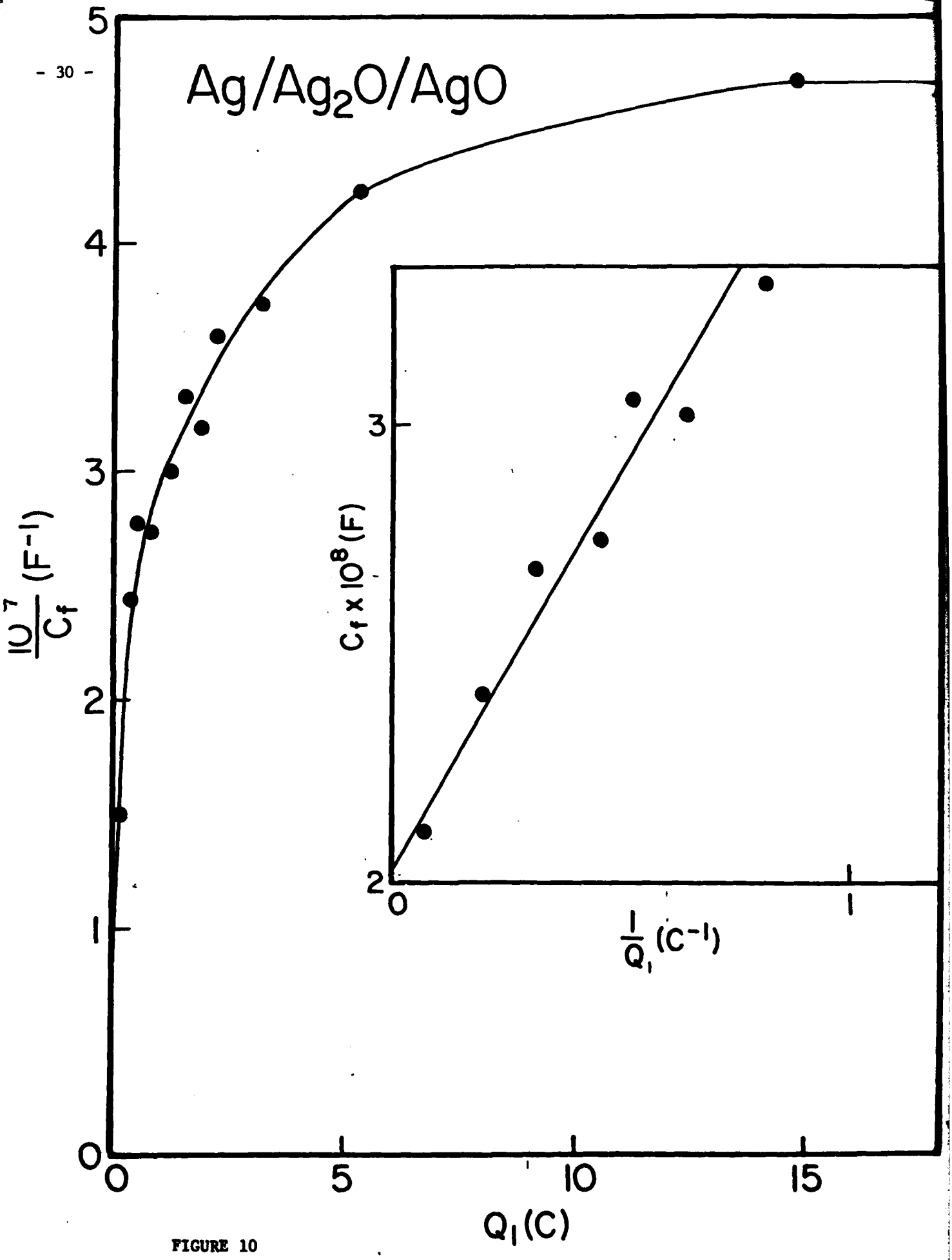

FIGURE 10

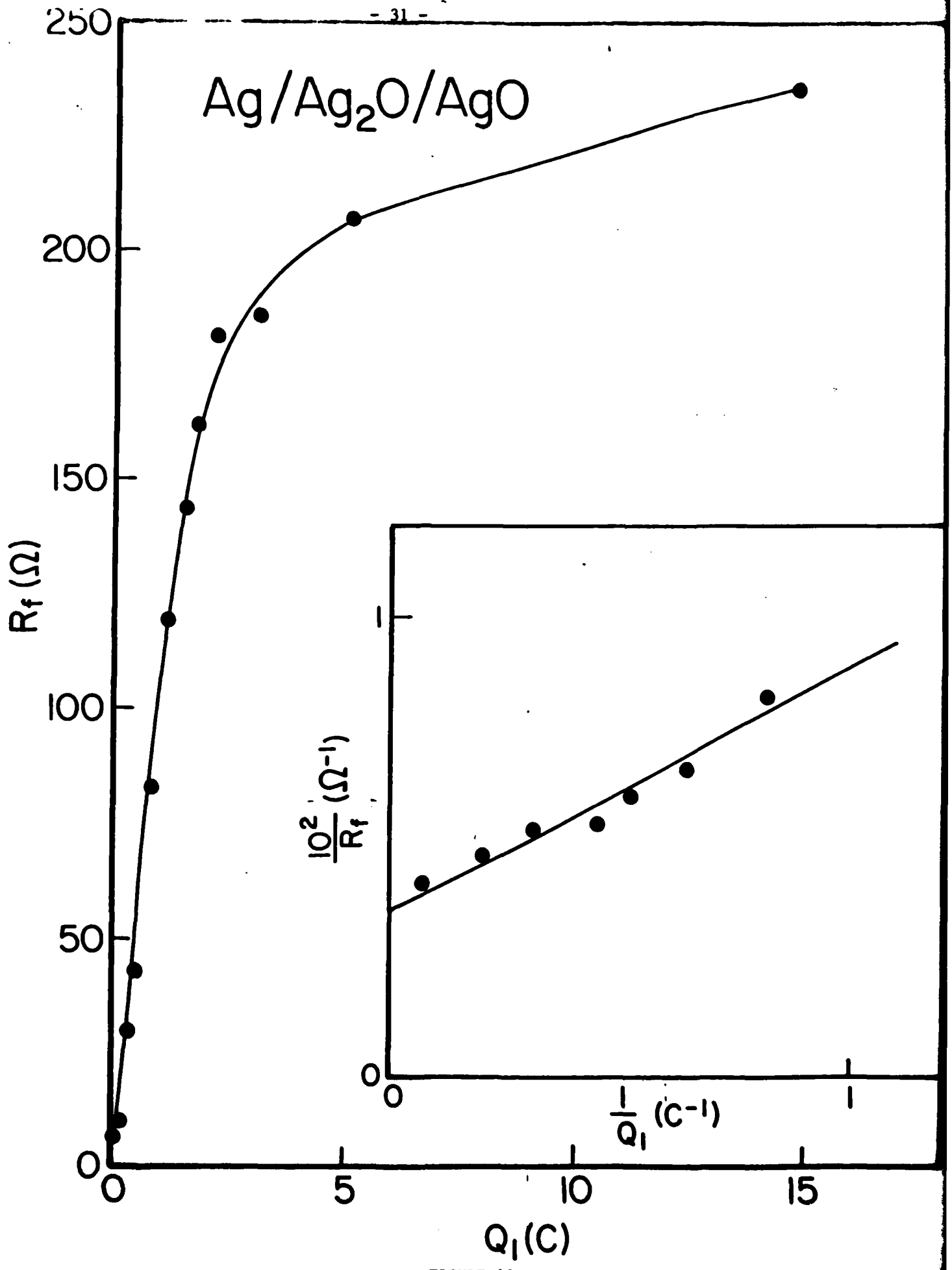
Ag/Ag2O/AgO
250
200
150
100
50
0
Rf (Ω)
0
5
10
15
Q1(C)
1
0
0
1
10²/Rf (Ω⁻¹)
1/Q1 (C⁻¹)

FIGURE 11

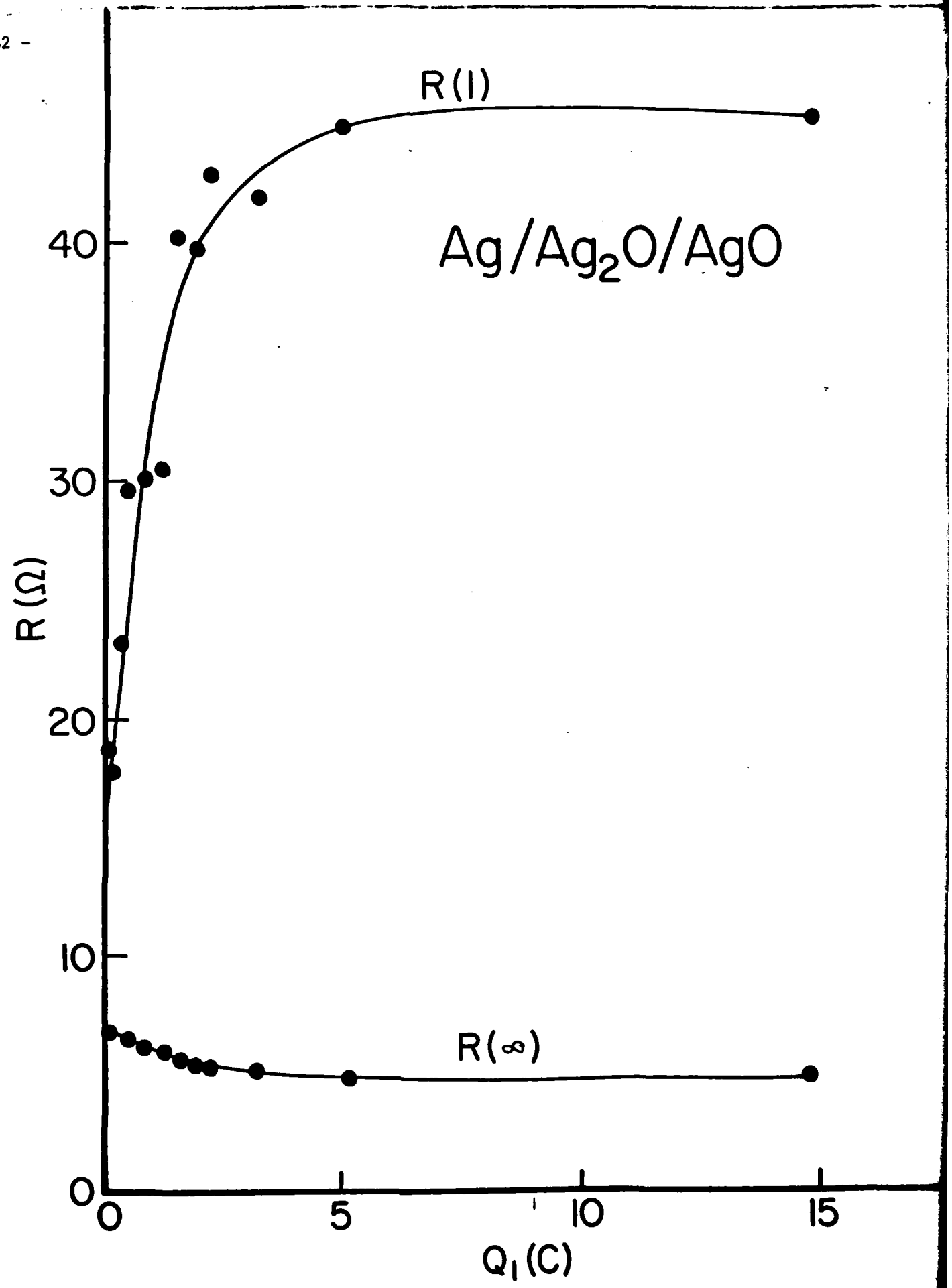

FIGURE 12

TECHNICAL REPORT DISTRIBUTION LIST, GEN

	No. Copies
Office of Naval Research Attn: Code 413 800 N. Quincy Street Arlington, Virginia 22217	2
ONR Pasadena Detachment Attn: Dr. R. J. Marcus 1030 East Green Street Pasadena, California 91106	1
Commander, Naval Air Systems Command Attn: Code 310C (H. Rosenwasser) Washington, D.C. 20360	1
Naval Civil Engineering Laboratory Attn: Dr. R. W. Drisko Port Hueneme, California 93401	1
Superintendent Chemistry Division, Code 6100 Naval Research Laboratory Washington, D.C. 20375	1
Defense Technical Information Center Building 5, Cameron Station Alexandria, Virginia 22314	12
DTNSRDC Attn: Dr. G. Bosmajian Applied Chemistry Division Annapolis, Maryland 21401	1
Naval Ocean Systems Center Attn: Dr. S. Yamamoto Marine Sciences Division San Diego, California 91232	1
Naval Ocean Systems Center Attn: Technical Library San Diego, California 92152	1
Naval Weapons Center Attn: Dr. A. B. Amster Chemistry Division China Lake, California 93555	1
Scientific Advisor Commandant of the Marine Corps Code RD-1 Washington, D.C. 20380	1
Dean William Tolles Naval Postgraduate School Monterey, California 93940	1
U.S. Army Research Office Attn: CRD-AA-IP P.O. Box 12211 Research Triangle Park, NC 27709	1
Mr. Vincent Schaper DTNSRDC Code 2830 Annapolis, Maryland 21402	1
Mr. John Boyle Materials Branch Naval Ship Engineering Center Philadelphia, Pennsylvania 19112	1
Mr. A. M. Anzalone Administrative Librarian PLASTEC/ARRADCOM Bldg 3401 Dover, New Jersey 07801	1

TECHNICAL REPORT DISTRIBUTION LIST, 359

Dr. Paul Delahay
Department of Chemistry
New York University
New York, New York 10003

Dr. P. J. Hendra
Department of Chemistry
University of Southampton
Southampton S09 5NH
United Kingdom

Dr. T. Katan
Lockheed Missiles and
Space Co., Inc.
P.O. Box 504
Sunnyvale, California 94088

Dr. D. N. Bennion
Department of Chemical Engineering
Brighma Young University
Provo, Utah 84602

Dr. R. A. Marcus
Department of Chemistry
California Institute of Technology
Pasadena, California 91125

Mr. Joseph McCartney
Code 7121
Naval Ocean Systems Center
San Diego, California 92152

Dr. J. J. Auborn
Bell Laboratories
Murray Hill, New Jersey 07974

Dr. Joseph Singer, Code 302-1
NASA-Lewis
21000 Brookpark Road
Cleveland, Ohio 44135

Dr. P. P. Schmidt
Department of Chemistry
Oakland University
Rochester, Michigan 48063

Dr. H. Richtol
Chemistry Department
Rensselaer Polytechnic Institute
Troy, New York 12181

Dr. E. Yeager
Department of Chemistry
Case Western Reserve University
Cleveland, Ohio 44106

Dr. C. E. Mueller
The Electrochemistry Branch
Naval Surface Weapons Center
White Oak Laboratory
Silver Spring, Maryland 20910

Dr. Sam Perone
Chemistry & Materials
Science Department
Lawrence Livermore National Lab.
Livermore, California 94550

Dr. Royce W. Murray
Department of Chemistry
University of North Carolina
Chapel Hill, North Carolina 27514

Dr. G. Goodman
Johnson Controls
5757 North Green Bay Avenue
Milwaukee, Wisconsin 53201

Dr. B. Brummer
EIC Incorporated
111 Chapel Street
Newton, Massachusetts 02158

Dr. Adam Heller
Bell Laboratories
Murray Hill, New Jersey 07974

Electrochimica Corporation
Attn: Technical Library
2485 Charleston Road
Mountain View, California 94040

Library
Duracell, Inc.
Burlington, Massachusetts 01803

Dr. A. B. Ellis
Chemistry Department
University of Wisconsin
Madison, Wisconsin 53706

TECHNICAL REPORT DISTRIBUTION LIST, 359

Dr. M. Wrighton
Chemistry Department
Massachusetts Institute
of Technology
Cambridge, Massachusetts 02139

Dr. B. Stanley Pons
Department of Chemistry
University of Utah
Salt Lake City, Utah 84112

Donald E. Mains
Naval Weapons Support Center
Electrochemical Power Sources Division
Crane, Indiana 47522

S. Ruby
DOE (STOR)
M.S. 6B025 Forrestal Bldg.
Washington, D.C. 20595

Dr. A. J. Bard
Department of Chemistry
University of Texas
Austin, Texas 78712

Dr. Janet Osteryoung
Department of Chemistry
State University of New York
Buffalo, New York 14214

Dr. Donald W. Ernst
Naval Surface Weapons Center
Code R-33
White Oak Laboratory
Silver Spring, Maryland 20910

Mr. James R. Moden
Naval Underwater Systems Center
Code 3632
Newport, Rhode Island 02840

Dr. Bernard Spielvogel
U.S. Army Research Office
P.O. Box 12211
Research Triangle Park, NC 27709

Dr. William Ayers
ECD Inc.
P.O. Box 5357
North Branch, New Jersey 08876

Dr. M. M. Nicholson
Electronics Research Center
Rockwell International
3370 Miraloma Avenue
Anaheim, California

Dr. Michael J. Weaver
Department of Chemistry
Purdue University
West Lafayette, Indiana 47907

Dr. R. David Rauh
EIC Corporation
111 Chapel Street
Newton, Massachusetts 02158

Dr. Aaron Wold
Department of Chemistry
Brown University
Providence, Rhode Island 02192

Dr. Martin Fleischmann
Department of Chemistry
University of Southampton
Southampton SO9 5NH ENGLAND

Dr. R. A. Osteryoung
Department of Chemistry
State University of New York
Buffalo, New York 14214

Dr. Denton Elliott
Air Force Office of Scientific
Research
Bolling AFB
Washington, D.C. 20332

Dr. R. Nowak
Naval Research Laboratory
Code 6130
Washington, D.C. 20375

Dr. D. F. Shriver
Department of Chemistry
Northwestern University
Evanston, Illinois 60201

Dr. Aaron Fletcher
Naval Weapons Center
Code 3852
China Lake, California 93555

TECHNICAL REPORT DISTRIBUTION LIST, 359

Dr. David Aikens
Chemistry Department
Rensselaer Polytechnic Institute
Troy, New York 12181

Dr. A. P. B. Lever
Chemistry Department
York University
Downsview, Ontario M3J1P3

Dr. Stanislaw Szpak
Naval Ocean Systems Center
Code 6343, Bayside
San Diego, California 95152

Dr. Gregory Farrington
Department of Materials Science
and Engineering
University of Pennsylvania
Philadelphia, Pennsylvania 19104

M. L. Robertson
Manager, Electrochemical
and Power Sources Division
Naval Weapons Support Center
Crane, Indiana 47522

Dr. T. Marks
Department of Chemistry
Northwestern University
Evanston, Illinois 60201

Dr. Micha Tomkiewicz
Department of Physics
Brooklyn College
Brooklyn, New York 11210

Dr. Lesser Blum
Department of Physics
University of Puerto Rico
Rio Piedras, Puerto Rico 00931

Dr. Joseph Gordon, II
IBM Corporation
K33/281
5600 Cottle Road
San Jose, California 95193

Dr. D. H. Whitmore
Department of Materials Science
Northwestern University
Evanston, Illinois 60201

Dr. Alan Bewick
Department of Chemistry
The University of Southampton
Southampton, S09 5NH ENGLAND

Dr. E. Anderson
NAVSEA-56Z33 NC #4
2541 Jefferson Davis Highway
Arlington, Virginia 20362

Dr. Bruce Dunn
Department of Engineering &
Applied Science
University of California
Los Angeles, California 90024

Dr. Elton Cairns
Energy & Environment Division
Lawrence Berkeley Laboratory
University of California
Berkeley, California 94720

Dr. D. Cipris
Allied Corporation
P.O. Box 3000R
Morristown, New Jersey 07960

Dr. M. Philpott
IBM Corporation
5600 Cottle Road
San Jose, California 95193

Dr. Donald Sandstrom
Department of Physics
Washington State University
Pullman, Washington 99164

Dr. Carl Kannewurf
Department of Electrical Engineering
and Computer Science
Northwestern University
Evanston, Illinois 60201

TECHNICAL REPORT DISTRIBUTION LIST, 359

Dr. Robert Somoano
Jet Propulsion Laboratory
California Institute of Technology
Pasadena, California 91103

Dr. Johann A. Joebstl
USA Mobility Equipment R&D Command
DRDME-EC
Fort Belvoir, Virginia 22060

Dr. Judith H. Ambrus
NASA Headquarters
M.S. RTS-6
Washington, D.C. 20546

Dr. Albert R. Landgrebe
U.S. Department of Energy
M.S. 68025 Forrestal Building
Washington, D.C. 20595

Dr. J. J. Brophy
Department of Physics
University of Utah
Salt Lake City, Utah 84112

Dr. Charles Martin
Department of Chemistry
Texas A&M University
College Station, Texas 77843

Dr. H. Tachikawa
Department of Chemistry
Jackson State University
Jackson, Mississippi 39217

Dr. Theodore Beck
Electrochemical Technology Corp.
3935 Leary Way N.W.
Seattle, Washington 98107

Dr. Farrell Lytle
Boeing Engineering and
Construction Engineers
P.O. Box 3707
Seattle, Washington 98124

Dr. Robert Gotscholl
U.S. Department of Energy
MS G-226
Washington, D.C. 20545

Dr. Edward Fletcher
Department of Mechanical Engineering
University of Minnesota
Minneapolis, Minnesota 55455

Dr. John Fontanella
Department of Physics
U.S. Naval Academy
Annapolis, Maryland 21402

Dr. Martha Greenblatt
Department of Chemistry
Rutgers University
New Brunswick, New Jersey 08903

Dr. John Wasson
Syntheco, Inc.
Rte 6 - Industrial Pike Road
Gastonia, North Carolina 28052

Dr. Walter Roth
Department of Physics
State University of New York
Albany, New York 12222

Dr. Anthony Sammells
Eltron Research Inc.
710 E. Ogden Avenue #108
Naperville, Illinois 60540

Dr. W. M. Risen
Department of Chemistry
Brown University
Providence, Rhode Island 02192

Dr. C. A. Angell
Department of Chemistry
Purdue University
West Lafayette, Indiana 47907

Dr. Thomas Davis
Polymer Science and Standards
Division
National Bureau of Standards
Washington, D.C. 20234